Pyrolysis of end-of-life polystyrene in a pilot-scale reactor: maximizing styrene production

Azd Zayoud[1,3], Hang Dao Thi[1], Marvin Kusenberg[1], Andreas Eschenbacher[1], Uros Kresovic[2], Nick Alderweireldt[2], Marko Djokic[1], Kevin M. Van Geem[1]

[1]Laboratory for Chemical Technology, Department of Materials, Textiles and Chemical Engineering, Ghent University, Gent 9052, Belgium;

[2]Indaver N.V. Belgium, Mechelen 2800, Belgium;

[3]Université Catholique de Louvain, Institute of Mechanics, Materials and Civil Engineering, 1348 Louvain-la-Neuve, Belgium

Highlights

- End-of-life polystyrene was pyrolyzed in CSTR under vacuum and atmospheric pressure
- Vacuum reduced the yield of styrene oligomers compared to atmospheric pressure
- Maximum styrene yield was 55.9 wt.% at 550 °C and 0.02 bara operating conditions
- Styrene dimers, trimers and tetramers were in detail quantified by GC × GC-FID/-MS

Graphical abstract

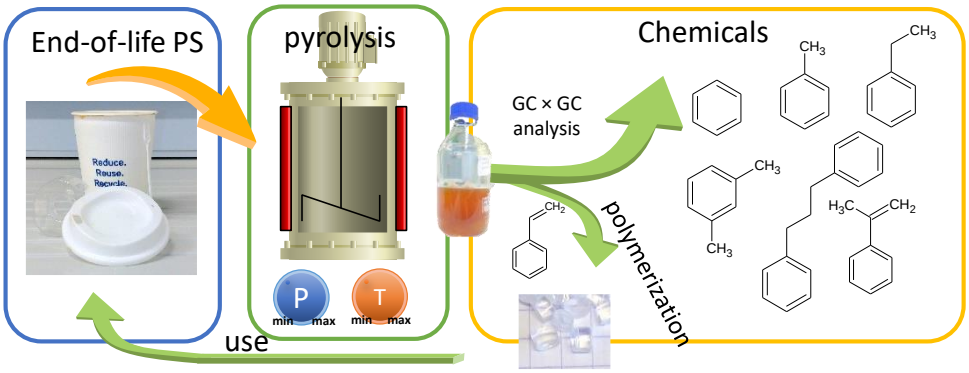

Abstract

Chemical recycling of polystyrene (PS) via pyrolysis is of great industrial, and academic interest, with styrene being the primary product of interest. To identify the optimal process conditions, the pyrolysis of end-of-life PS was studied in a pilot-scale unit consisting of an extruder, and a continuous stirred tank reactor (CSTR). The PS was pyrolyzed with continuous feeding at a pressure range from 0.02 to 1.0 bara, and a temperature range from 450 to 600 °C, giving primarily styrene, other mono-aromatics, and oligomers. The comprehensive two-dimensional gas chromatography (GC × GC) coupled with flame ionization detector (FID), and time-of-flight mass spectrometer (ToF-MS) as well as GC with thermal conductivity detector (TCD) were used to characterize the liquid, and gaseous products exhaustively.

The styrene yield increased from 36 wt.% at 1.0 bara, and 450 °C to 56 wt.% at 0.02 bara, and 550 °C. Working under a vacuum enhanced the styrene recovery at all corresponding temperature levels. The yield of benzene, toluene, ethylbenzene, and xylene (BTEX) increased from 4 wt.% at 450 °C, and 0.02 bara to 17 wt.% at 450 °C, and 1.0 bara. The experimental results have been used in a mathematical model that can explain the combined effect of temperature, and pressure on the yield of the primary products. The present work illustrates the potential of a continuous pyrolysis process for end-of-life PS, and paves the way for this technology to be rapidly transferred from mere laboratory use to industrial processes in the circular (petro-) chemical industry.

Keywords: pyrolysis, waste plastic, continuous process, polystyrene, CSTR, mathematical optimization

1 Introduction

The steadily increasing plastics production due to a continuously growing global demand exacerbates the end-of-life plastics problem. In 2018, the world production exceeded 350 million metric tons, where the European production share was around 17% (Garside, 2019). The intensive use of plastics has put the spotlight on how to resolve the end-of-life plastic problem (PlasticsEurope, 2018). Additionally, China, and India banned the import of end-of-life plastics (Brooks et al., 2018). As a result, treating end-of-life plastics domestically becomes unavoidable for many countries. In Europe, the target is set to reuse, and recycle 60 % of all plastic packaging by 2030, and 100% of all plastic packaging will be either reused, recycled, or recovered by 2040 (PlasticsEurope, 2019a).

PS is one of the main demanded polymers, and subsequently one of the major end-of-life plastic types (PlasticsEurope, 2019b). And PS pyrolysis has been studied intensively during the past decades. However, to date, the reported studies in open literature have been focused on processing virgin PS and ultra-pure waste PS but not (contaminated) end-of-life PS. Madorsky and Straus were one of the first to perform PS pyrolysis experiments in a laboratory-scale batch reactor at vacuum pressure and a temperature range from 340 to 420 °C; these researchers reported a maximum styrene recovery of 42 wt.% at 420 °C (Madorsky and Straus, 1948). In 1981, Ogino and Nagy used a micro-pyrolyzer to process PS at vacuum pressure and a temperature range between 400 and 500 °C, achieving a high styrene yield of 84.5 wt.% (Ogino and Nagy, 1981). Using a laboratory-scale fixed bed reactor, Achilias et al. pyrolyzed PS at 510 °C and obtained a styrene selectivity of 63.9 wt.% in their condensed liquid product, which implies an overall styrene yield of 58.7 wt.% (Achilias et al., 2007). Mo et al. applied a response surface method (RSM) to maximize the styrene recovery using a laboratory-scale

65 semi-batch horizontal tube furnace at atmospheric pressure and found a maximum styrene
66 yield of 60.9 wt.% at 490 °C (Mo et al., 2014). A microwave laboratory-scale reactor was used
67 to pyrolyze PS in a temperature range from 464 to 678°C, and reported a styrene yield of 66.0
68 wt.% (Undri et al., 2014). Similarly, Bartoli et al. performed PS pyrolysis with a microwave
69 laboratory-scale reactor at vacuum pressure and a temperature range of 301-536 °C and
70 reported a styrene yield of 60.6 wt.% (Bartoli et al., 2015). The earliest works by Kim et al.
71 using laboratory-scale reactors proved the concept of recovering monomers of PS through a
72 pyrolysis process (Kim et al., 1999). However, most of the previous works used either batch or
73 manual feeding modes (Chauhan et al., 2008; Liu et al., 2000; Park et al., 2003; Williams and
74 Williams, 2010). The batch and manual feeding modes have inherent downtime, high
75 operating cost, and product variability, as a result, these batch processes and manual feeding
76 reactors have little potential to be scaled up (Qureshi et al., 2018). Anyhow, these preliminary
77 works have paved the way for advancing the experimental end-of-life plastics pyrolysis works.

78 Further investigation of the PS pyrolysis process with continuous feeding is required since only
79 a few PS pyrolysis experiment works were performed in continuous mode (Ando et al., 1974;
80 Kaminsky et al., 2004; Park et al., 2020).

81 Even though data is scarce, PS pyrolysis gains momentum on an industrial scale, with several
82 demonstration projects being announced (PolystyreneLoop, 2021; Pyrolyze.B.V., 2021;
83 Smalley, 2019; Victory, 2020). Until today, PS pyrolysis in a CSTR with continuous feeding has
84 not been implemented on an industrial scale yet. Instead, reactors such as a twin-screw and a
85 microwave reactor have been used to process PS (Agilyx, 2020; Doucet, 2020; Doucet et al.,
86 2016; Qureshi et al., 2019). According to classical chemical engineering principles, scaling up
87 step by step of the continuous processing capacity is considered best practice. Therefore,

88 further investigations on PS pyrolysis in a CSTR with continuous feeding are advised before
89 developing and building an industrial size plant. The CSTR is a robust reactor type, offering the
90 flexibility of operating at different temperatures and pressure levels, *viz.* vacuum, atmospheric
91 pressure and elevated pressure. Based on this flexibility in operating conditions, this reactor
92 type was selected for the present work. An additional advantage is that it facilitates the
93 processing of a broad range of plastics types such as PE, PP, PS, and mixed plastic waste.

94 Besides the lack of studies on PS pyrolysis in continuous feeding mode and operating under
95 vacuum, there is limited knowledge about the detailed composition of the oligomers of
96 styrene formed during the pyrolysis of PS. With more advanced analytical techniques, it is
97 possible to gain new insights into PS pyrolysis and the impact of the process conditions on
98 monomer and oligomer formation. In particular, under vacuum, it is expected that more
99 styrene can be formed because secondary reactions are minimized. In the open literature, the
100 PS pyrolyzate analysis was only carried out using one-dimensional gas chromatography (1D-
101 GC) with typically either a thermal conductivity detector (TCD), a flame ionization
102 detector (FID), or a time of flight mass spectrometry detector (TOF-MS) (Kaminsky and Franck,
103 1991; Kim et al., 1999; Ogino and Nagy, 1981; Park et al., 2003; Park et al., 2020; Williams and
104 Williams, 2010). In the characterized pyrolyzate, the unidentified compounds ranged between
105 7 and 18 wt.%, possibly because of insufficient identification with databases and limitations
106 of the sampling system (Artetxe et al., 2015; Kaminsky et al., 2004; Park et al., 2020). Kaminsky
107 et al. identified 12 PS pyrolyzate compounds (Kaminsky, 2021; Kaminsky et al., 2004) and Undri
108 et al. quantified the compounds with a concentration ≥0.2% (Undri et al., 2014).
109 Comprehensive two-dimensional gas chromatography (GC × GC) (Dalluge et al., 2002) can be
110 beneficial for the quantitative analysis because of its intrinsic higher sensitivity (Dijkmans et

al., 2015; Phillips and Beens, 1999). The most advanced study -for detailed compositional characterization of plastic waste pyrolysis oil- considered GC × GC coupled to multiple detectors such as FID, TOF-MS, a sulfur chemiluminescence detector (SCD), and nitrogen chemiluminescence detector (NCD), enabling the quantification of impurities (Toraman et al., 2014).

The primary aim of the present study was to improve the understanding of the effect of temperature and pressure on the continuous pyrolysis process of end-of-life PS feedstock which was obtained from industrial scale sorting plant. This was performed in a CSTR pilot-scale continuous feeding unit. Particular attention was paid to the detailed quantification and identification of the formed oligomers, the pyrolyzate was analyzed in detail using the state of the art comprehensive two dimensional GC × GC-FID/-MS. Experiments were conducted at three pressure levels (0.02, 0.5, and 1.0 bara), and four temperature levels (450, 500, 550, and 600 °C); interestingly, the vacuum pressure was found to have an insignificant effect on the pyrolyzate yield, but a noteworthy effect on the composition of the pyrolyzate products. The maximum styrene and maximum liquid pyrolyzate yields were obtained at vacuum pressure (0.02 bara) and an operating temperature of ~550 °C. These findings can be used for optimizing the operating conditions of an industrial plant. The obtained products were analyzed using a comprehensive set of analytical techniques. The obtained experimental results were interpolated using a mathematical model to predict the optimal operating conditions.

2 Materials and Methods

2.1 Materials

End-of-Life PS (Coolrec, Belgium) was used as a feedstock for the pyrolysis experiments. The end-of-life PS was collected, washed, shredded, and granulated. The composition of the used waste fractions has been estimated (Roosen et al., 2020a), and is given by 94.2 % (E)PS, 0.2 % PET, 1.2 % PE, 0.5 % EVOH, 0.5 % PA, 0.3 % PUR, and 3.0 % paper; and the weight-based elemental composition (CHNS/O) of the end-of-life PS is given by 86.6 % C, 8.2 % H, 0.5 % N, <level of detection (LOD) S, 2.7% O and 2.0 % metal and halogen contents (Roosen et al., 2020a). Additionally, the ultimate analysis was carried out for pyrolyzate products [e.g. (Exp. 4)], the measured CHNS/O is given by 86.3 % C, 7.7 % H, 0.6 % N, <LOD S, 5.3 % O and other compounds. Carbon disulfide, with a purity of 99.9% (Sigma-Aldrich, Belgium), was used as a solvent to dissolve the PS pyrolyzate before the GC × GC analysis. 3-Chlorothiophene, procured with a purity of 97% (Sigma-Aldrich, Belgium), was used as an internal standard in GC × GC analysis. Benzene, toluene, and styrene with a purity of ≥99% (Acros Organics, Belgium) were used for external calibration. Analytical gasses (nitrogen, helium, oxygen, and hydrogen) used for GC × GC had a minimum purity of 99.999% (AirLiquide, Belgium). The 4-tert-Butylcatechol inhibitor with a purity of ≥99.0% (Sigma-Aldrich, Belgium) was added to the pyrolyzate samples to avoid auto-polymerization.

2.2 Experimental apparatus and procedure

2.2.1 Pyrolysis pilot unit

The PS pyrolysis experiments were performed using an in-house developed continuous pyrolysis pilot-scale unit at the Laboratory for Chemical Technology (LCT, Ghent University,

Ghent 9052, Belgium). As shown in Figure 1, the pyrolysis unit consists of three main sections. In the feeding section, a LabTech single screw extruder (1) (Model: LE25-30/CV, Thailand) with a feeding rate range of 0.1-10 $kg \cdot h^{-1}$, and four dedicated heating zones are used to pre-heat and melt the granulated plastic feedstock and to feed it to the reactor. The extruder's outlet is connected to the reactor's inlet by a heated transfer line; more information on the extruder's specifications can be found in the (supplentary information).

In the reaction section, a Parr reactor (Model: 4584, U.S.A) is used for pyrolysis. The reactor has a volume of 5.7 L (1.5 gallons) and the heat is provided using a heating jacket. The reactor conditions are controlled through a PC (3) using SpecView software and a PID controller. The reactor is also equipped with three K-type thermocouples, a stirrer, shaft magnetic coupling, a manometer, and a pressure transducer. A nitrogen bottle of ≥99.99% purity (4) (AirLiquide, Belgium) is connected to the reactor for purging before the experiment and the nitrogen flow is controlled through a volume flow controller (5) (KROHNE, MD: 2018, Germany).

In the condensation section, three condensers (6) operated in series captured the pyrolyzate and the temperature of these condensers is controlled by using an external LAUDA cooler (7) (RE 420 G, Germany). Each condenser set consists of three valves: **a)** valves (Figure 1, v-201, v-188, and v-178) between the condensers and the collecting vessels, **b)** valves for releasing pressure (v-202, v-179, and v-183) into the ventilation line in case of non-atmospheric experiments and **c)** valves (v-203, v-191, and v-190) beneath the collecting vessel to sample products. The temperature of the first, second, and third condensers are set at -10 °C. The outlet of the third condenser is connected to a three-way valve which directs the off-gasses either to a back-pressure regulator (Figure 1, 8) (EQUILIBAR, U.S.A) or a vacuum pump (Figure 1, 9) (KNF, SC 920G, Germany). Depending on the desired pressure level, either the vacuum

pump or the back-pressure regulator is used to reach vacuum or atmospheric pressure in the reactive, and condensation sections. Subsequently, the outflow of the vacuum pump or the back-pressure regulator (Figure 1, PR-010) is forwarded to the knock-out drum to capture any remaining pyrolyzate. A sampling port was used to collect the gas sample using a Tedlar bag. A drum-type gas flowmeter (Figure 1, 10) (Ritter, TG3/1-1bar, Germany) is employed to measure the volume of the gaseous products before venting them. All pipes, and fittings are made of stainless steel 316 (Swagelok, U.S.A.).

2.2.2 Operational procedure and sampling

At the beginning of an experiment, the apparatus was cleaned and tested for leak-tightness. The apparatus was flushed with N_2 flow for a sufficiently long time to ensure an inert atmosphere in the unit. The temperature of the condenser's cooler was set at a level of -10 °C. The temperature of the extruder's heaters was set at ≤ 300 °C to melt and feed PS without degradation of the PS in the extruder and the four heaters of the extruder were set from the inlet side to the outlet side at 150, 250, 300, and 300 °C, respectively. This temperature profile of the extruder was applied for all experiments. The heat tracing of the reactors' inlet and outlet lines was maintained at 300°C.

Next, the pre-cleaned reactor was pre-heated to the desired temperature level. As soon as the temperature at the head of the reactor exceeded the melting point ($PS_{m.p.}$=240 °C) of the plastics feedstock by 50 °C, i.e. at 290 °C, the plastic feeding was started by turning on the extruder's motor gradually. The feeding rate of the PS feedstock was calibrated once by measuring the required time to feed 1 kg of plastics at three rotational speed settings of the extruder's screw at 10, 20, and 30 revolutions per minute (R.P.M). The R.P.M. was increased gradually until reaching the feeding rate of 1 $kg \cdot h^{-1}$. The rotational speed of the reactor stirrer

199 was set at 100 R.P.M. to mix the melted plastics in the reactor and to enhance the heat transfer
200 (Figure S1). In each experiment, 4 kg of end-of-life PS feedstock were pyrolyzed. The liquid
201 pyrolyzate was cooled down to -10 °C in the condensation section that comprises 3 "tube in
202 tube" heat exchangers and was collected with an interval of 30 min. The sampling time interval
203 was assumed to be long enough to minimize pressure fluctuations in the reactor. The liquid
204 pyrolyzate samples of each experiment were accumulated in one aluminum bottle and at the
205 end of the experiment, the overall collected liquid pyrolyzate was weighed on a scale
206 (Sartorius ENTRIS8201-1S, Germany). The weight of the gas products was calculated by
207 multiplying the measured volume by the density of the gaseous products. On the one hand,
208 the gaseous product volume was measured using the wet Ritter flowmeter during the entire
209 experiment. On the other hand, the detailed composition of the gaseous products was
210 analyzed using 1D GC-FID/TCD (so-called refinery gas analyzer (RGA)) that has already been
211 explained in detail (Djokic et al., 2017). The analysis was triplicated and the density of the
212 gaseous samples was determined based on the compounds' wt.% in the gas sample and the
213 pure components' density. The char yield was calculated by difference. All product yields in
214 the present work were calculated based on the mass of PS fed into the reactor.

215 The mean residence time ($t_{res.}$) is calculated using Equation 1 (Murata et al., 2004).

$$Residence\ time\ [min] = \frac{\text{reactor content [g]}}{\text{feeding rate } [\frac{\text{g}}{\text{min}}]} \qquad \textit{Equation 1}$$

216 For each experiment, the reactor content was calculated at each time of sampling by the
217 difference between the fed PS into the reactor and the collected pyrolyzate products,
218 subsequently the $t_{res.}$ was calculated (Equation 1). At the end of each experiment, the average
219 of $t_{res.}$ was calculated.

After feeding 4 kg of PS, the feeding was stopped; the pyrolyzate was sampled and the temperature in the reactor was increased up to 600 °C for 30 min to remove all hydrocarbon residues in the reactor before shutting off the coolers and heating elements. The sampled pyrolyzate during the elevated temperature (600 °C) was used only for the mass balance calculation. The rest of the collected samples of each experiment were stored in one aluminum bottle from which the GC × GC sample was taken, and a 4-tert-Butylcatechol (TBC) inhibitor was added to prevent the styrene auto-polymerization.

2.3 Experimental conditions

Seven PS pyrolysis experiments were design and performed (see supplementary information). At pressure level of 0.02 bara, three experiments, namely Exp. 1, Exp. 2, and Exp. 3, were performed, at three different temperatures of 450 °C, 550 °C, and 600 °C, respectively. At a pressure of 1.0 bara, the three experiments Exp. 5, Exp. 6, and Exp. 7 were performed at temperatures of 450 °C, 550 °C, and 600 °C, respectively. The 4^{th} experiment (Exp. 4) was operated at a temperature of 500 °C, and a pressure of 0.5 bara. The latter experiment constitutes the midpoint of the operating conditions of Exp. 1, Exp. 2, Exp. 5, and Exp. 6. The 4^{th} Exp. was performed to assess the linearity of the yield compositions response with the operating pressure, and temperature. Furthermore, collecting the samples under steady-state conditions was checked, and assured by collecting, and analyzing three samples after 30, 60, and 90 min. The feeding rate was kept constant for all experiments at 1 $kg{\cdot}h^{-1}$ and 4 kg of polystyrene was fed for each condition.

2.4 Analytical methods

For the qualitative analysis, a GC × GC-TOF-MS was used to identify unknown compounds in the liquid pyrolyzate. GC × GC-FID was used to quantify the liquid pyrolyzate composition.

Moreover, the composition of the non-condensed off-gasses was analyzed using a 1D GC-FID/TCD (RGA), which is explained in detail in previous work (Djokic et al., 2017).

2.4.1 Sample preparation

Two analytes of each pyrolyzate sample were prepared for analysis using GC × GC-FID and GC × GC-ToF-MS. The first analyte was prepared to quantify the highest concentrated compounds, namely, toluene, alpha-methylstyrene, and styrene. The first analytes were prepared by adding 40 wt.% of 3-chlorothiophene to measure the compounds of high concentration. External calibration was performed to determine the response factor of the major compounds such as benzene, toluene, and styrene using high purity chemicals (Sigma-Aldrich, Belgium, purity 99.8%). The second analytes were prepared by adding 5 wt.% of 3-chlorothiophene internal standard, for quantification of the compounds present at lower concentrations. In order to decrease the viscosity and inhomogeneity of the samples, carbon disulfide (CS_2) was used to dilute the sample (1:1 volumetric ratio).

2.4.2 GC × GC-FID / TOF-MS setup

Two Thermo Scientific TRACE GC × GC instruments (Interscience, Belgium) equipped with an FID detector and a TOF-MS detector (Interscience, Belgium) were used to analyze all samples. The GC × GC was equipped with a dual-stage cryogenic (liquid CO_2) modulator, and a programmable temperature vaporization (PTV) injector (Interscience, Belgium). A non-polar RTX®-1 PONA column (Restek, 50 m × 0.25 mm × 0.5 µm) was used as the first dimension column, while a polar BPX-50 column (SGE Analytical Science, 2 m × 0.15 mm × 0.15 µm) was used as the second-dimension column. The PTV temperature was increased from 40 °C up to the maximum temperature of 370 °C with a rate of 15 °C·s^{-1}. The initial GC oven temperature was 40 °C, and it was increased up to 370 °C at a rate of 3 °C·min^{-1} and held for 600 sec with

a set modulation time of 6 sec. The helium carrier gas flows were set to 2.1 mL·min^{-1} and 2.3 mL·min^{-1} for FID and TOF-MS analysis, respectively (Beens et al., 2005).

Data acquisition and quantification: Xcalibur™ Software (Thermo Scientific, U.S.A) was used for the acquisition and processing of GC × GC-ToF-MS data. For the GC × GC-FID data, Thermo Scientific's Chrom-Card data system was used. The raw GC × GC-FID data was exported as *.cdf* file and subsequently processed by GC Image software (Zoex Corporation, U.S.A). The obtained peaks were identified using ToF-MS spectra in comparison with the spectra available in the MS libraries. The blob names and peak volumes were exported as *.csv* files which were subsequently post-processed. In previous work, the quantification procedure was described in detail by Dijkmans et al. (Dijkmans et al., 2015).

The weight fraction wt.%$_i$ of each compound (*i*) was assigned based on the known weight fraction wt.%$_{IS}$ of internal standard (3-chlorothiophene) using the following equation:

$$wt.\%_i = \frac{f_i \,.V_i}{f_{IS}.V_{IS}}.wt.\%_{IS} \qquad \textit{Equation 2}$$

f_i is the relative response factor of compound *i*, V_i is the peak volume of compound *i*, f_{IS} is the relative response factor of the internal standard, and V_{IS} is the peak volume of the internal standard. The relative response factor was calculated with respect to methane as follows:

$$f_i = \frac{M_i[kg/mol]}{M_{CH_4}[kg/mol].N_{C,i}} \qquad \textit{Equation 3}$$

where M_i is the molar mass of compound *i*, M_{CH4} is the molar mass of methane and $N_{C,i}$ is the carbon number of compound *i* (Beens et al., 1998).

The response factors f_i of some compounds (benzene, toluene, and styrene) were determined experimentally. The experimentally measured relative response factors of the mono-aromatic

compounds were 90.5% of the calculated response factor based on the effective carbon number. The relative response factors of the remaining compounds in the samples were calculated using the effective carbon number approach used by Djokic et al. (Djokic et al., 2013).

2.5 Data visualization and interpolation

The Akima mathematical method of interpolation was used for the set of experimental data points (Akima, 1970, 1974, 1978). The z value is interpolated with a bivariate fifth-degree polynomial Equation 4.

$$z(x,y) = \sum_{i=0}^{5} \sum_{j=0}^{5-i} a_{ij} x^i y^j \qquad \textit{Equation 4}$$

The interpolation was performed to visualize the effect of the operating parameters pressure (x), and temperature (y) over the pyrolyzate product compounds (z). For each product type, the experimental pyrolyzate results at all operating pressure and temperature levels are used to interpolate points of a mesh of 15 × 15 size. This mathematical model has been used to further interpret the data.

3 Results and discussion

3.1 Mass balance

The yields of the main product fractions obtained using the CSTR continuous pyrolysis reactor are shown in Figure 2. The major product fraction was liquid pyrolyzate with a weight percentage varying between 88.5 and 94.1 wt.%. Under vacuum (0.02 bara) and at temperatures of 450, 550 and 600 °C (Exp. 1, Exp. 2 and Exp. 3), the liquid pyrolyzate yields improved insignificantly at 0.02 bara and it was 91.6, 94.5, and 88.9 wt.% compared to 90.4,

94.1 and 88.5 wt.% at 1.0 bara at the corresponding temperatures (Exp. 5, Exp. 6 and Exp. 7). Our experimental results show a trend of increasing liquid pyrolyzate yields with an increased temperature up to 550 °C. An increased temperature above 550 °C led to lower liquid pyrolyzate due to favored secondary reactions at the higher temperature. Similar behavior was observed for PS pyrolysis experiments in a conical spouted bed (Artetxe et al., 2015; Karaduman et al., 2001) and this behavior was found as well for PS pyrolysis experiments using a fluidized bed reactor at a temperature range from 505 to 782 °C (Park et al., 2020). This trend can be attributed to reactions of contrary effects that influence the pyrolysis liquid yield recovery: on the one hand, the end-chain β-scission and polymer volatilization enhance the liquid yield recovery with increasing temperature (Murata et al., 2004). On the other hand, the secondary reactions decrease the pyrolysis liquid yield and stimulate gaseous and char formation with increasing temperature (Artetxe et al., 2015; Liu et al., 2000).

In the studied pressure range (0.02-1.0 bara), the lower pressure (0.02 bara) has an insignificant effect on the yield of the liquid pyrolyzate compared to 1.0 bara at all corresponding temperature levels. In contrast, the vacuum pressure affects significantly the selectivity of the compounds in the liquid yield (see section 3.3).

At the atmospheric pressure level, the total yield of off-gasses is increased from 0.8 at 450 °C (Exp. 5) to 1.5 wt.% at 550 °C (Exp. 6) and finally up to 3.2 wt.% at 600 °C (Exp. 7), the latter as a result of the enforced secondary over-cracking reactions. A similar trend was found at a pressure level of 0.02 bara compared to atmospheric pressure, but with a lower yield at the corresponding temperature levels, which is attributed to the shorter $t_{res.}$ at lower operating pressure.

At the pressure level of 0.02 bara, in contrast with liquid pyrolyzate, the char formation decreased from 6.7 wt.% at 450 °C to 3.2 wt.% at 550 °C, then again increased to 8.8 wt.% at 550 °C. Likewise, at the atmospheric pressure level, the char formation decreased from 8.9 wt.% at 450 °C to 4.4 wt.% at 550 °C, then again increased to 8.3 wt.% at 550 °C. A similar trend was observed by Park et al. and the experimental results of PS pyrolysis in a circulating fluidized bed show a decrease of the char formation before increasing again in a temperature range from 515 to 782 °C (Park et al., 2020). The char formation trend behaves oppositely relative to the pyrolysis liquid formation trend. Enhanced end-chain β-scissions and polymer volatilization reactions at increased temperature are responsible for the increased liquid pyrolysis products and decrease the char formation. On the other hand, the secondary cracking reactions become dominant at temperatures higher than 550 °C, which leads to increased gas yield and char formation and thus a lower liquid yield. The lower pressure minimizes the t_{res}., which mitigates the secondary cracking reactions; as a result, the liquid yield increases.

The operating pressure in the studied range had a lower influence on the product yields compared to the operating temperature; In all cases, at operating levels of 0.02 and 1.0 bara, the difference between the product yields was ±1.3 wt.% at the corresponding temperature level. As an example, at 550 °C, liquid yields at 0.02 and 1.0 bara were 94.5 and 94.1 wt.%, respectively. At the mid-point (Exp. 4, 500 °C and 0.5 bara), the pyrolysis liquid product yield matched 99% of the product yield averages of Exp. 1 (450 °C, 1.0 bara), 2 (550 °C, 0.02 bara), Exp. 5 (450 °C, 1.0 bara) and Exp. 6 (550 °C, 1.0 bara).

3.2 The residence time

The residence time ($t_{res.}$) influences the rate of secondary reactions and the shorter $t_{res.}$ leads to a lower rate of secondary reactions. At both pressure levels, viz. 0.02 and 1.0 bara, the $t_{res.}$ decreases with increased temperature. This observation can be explained by enhanced devolatilization and β-scission reactions (Artetxe et al., 2015; Madorsky, 1952; Murata et al., 2002). At 0.02 bara, the $t_{res.}$ decreased from 39.0, 16.0 to 15.6 min at 450, 550 and 600 °C, respectively. Compared to a reactor pressure of 0.02 bara, the trend was found as well at the 1.0 bara level, but higher at the corresponding temperature and decreased from 47.8, 41.6, and 18.6 min at 450, 550, and 600 °C, respectively. The operating temperature has a higher influence compared to the operating pressure on the $t_{res.}$ (see supplementary information). Murata et al. found a similar trend of decreasing $t_{res.}$ with the decreased pressure, however, the authors reported a more pronounced effect in their study due to the higher pressure range from 1.0 bara to 8.0 bara; Murata et al. stated that the degradation and volatilization reactions were a function of temperature, pressure and $t_{res.}$ (Murata et al., 2004). To calculate the $t_{res.}$ (Equation 1), the reactor content was estimated by weight difference between the fed PS into the reactor and the sampled pyrolyzate; this procedure can be enhanced further by the addition of a sensor to measure the reactor content in future experimental work.

3.3 Composition of pyrolyzate

Comprehensive GC × GC-FID analysis: in all cases, over 95 wt.% of the collected liquid fractions were quantified and the dominant compound was styrene. The carbon number of the detected compounds ranged from C_3 to C_{24}. The GC × GC-FID analyses results showed on average major amounts of mono-aromatics (62 wt.%), di-aromatics (13 wt.%), and tri-aromatics (7 wt.%) (Table 1), as well as small amounts of tetra-aromatics and aliphatics.

Figure 3 shows the comprehensive GC × GC-FID chromatogram of the end-of-life PS pyrolyzate (Exp. 1). The chromatogram shows five aromatic groups (mono-aromatics, di-aromatics, tri-aromatics, tetra-aromatics, and penta-aromatics) and the aliphatic group. The key compounds of end-of-life PS pyrolyzate are indicated in the chromatogram (Figure 3). The major compounds of the mono-aromatic groups were **(c)** Toluene **(e)** Ethylbenzene **(f)** Styrene **(j)** Alpha-methylstyrene. The dominant compounds of the poly-aromatic groups were **(q)** Bibenzyl **(r)** 1,2-Diphenylpropane **(t)** 1,3-Diphenylpropane **(u)** 2,4-Diphenyl-1-butene **(v)** 1,3-Diphenylpropene **(w)** 2,4-Diphenyl-1-pentene **(x)** 2,4,6-triphenyl-1-hexene **(y)** 1,2,4-Triphenylbenzene. The polypropylene contamination in the PS feedstock is detected by identifying the 2, 4, 6, 8-tetramethyl-1-undecene in the pyrolyzate—one of the major fingerprint compounds from polypropylene pyrolysis (Soják et al.). Additionally, small amounts of compounds with oxygen and/or nitrogen atoms were detected, such as Benzene-acetamide, which is attributed to the impurity of the end-of-life PS feedstock.

3.3.1 Composition of pyrolyzate at the atmospheric pressure

Figure 4 shows the yield of the four major groups found in the liquid pyrolyzate: i) styrene, ii) other mono-aromatics, iii) poly-aromatics (PA) and iv) aliphatic compounds. In all investigated process conditions, the major compound of the pyrolyzate was styrene. The yield of styrene increased from 35.7 wt.% at 450 °C to 41.2 wt.% at 550 °C and reached 43.2 wt.% at 600 °C. Liu et al. studied the effect of temperature on polystyrene pyrolysis yield from 450 °C to 700 °C and found that the styrene yield increased with the increased temperature to reach a certain temperature point (600 °C) at which the styrene concentration was maximum (78.8 wt.%), then decreased to 60 wt.% at 700 °C (Liu et al., 2000). This trend can be attributed to reactions of contrary effects that influence the styrene production: on the one hand, the

394 styrene concentration increases because of the enhanced depolymerization rate and end-
395 chain β-scission reactions with the increased operating temperature (Artetxe et al., 2015;
396 Madorsky, 1952; Murata et al., 2002). On the other hand, the secondary reactions decrease
397 the styrene concentration and stimulate gases and char formation with increasing
398 temperature (Artetxe et al., 2015; Liu et al., 2000). In this work, the styrene concentration
399 increased with the increased temperature until reaching the maximum operating temperature
400 of 600 °C. The temperature point of maximum styrene is assumed to lie beyond the maximum
401 studied temperature level (600 °C). The temperature level was restricted because it became
402 difficult to sustain a stable operating temperature at higher levels.

403 At atmospheric pressure, the yield of other mono-aromatics (excluding styrene) decreased
404 from 25.1 wt.%, 25.0 wt.% to 22.9 wt.% with increased temperature from 450 °C, 550 °C to
405 600 °C, respectively, in favor of increased styrene yields (Figure 4).

406 On the other hand, the yield of benzene, toluene, ethylbenzene, and xylenes (BTEX) decreased
407 from 17.1 wt.% at 450 °C (Exp. 5) to 15.6 wt.% at 550 °C and 600 °C (Exp. 6, Exp. 7). Similarly,
408 the alpha-methylstyrene decreased from 6.1 wt.% at 450 °C (Exp. 5), 6.0 wt.% at 550 °C (Exp.
409 6) to 4.4 wt.% at 600 °C (Exp. 7) (Figure 4 and Figure 5). The decrement of these mono-
410 aromatics yields is attributed to the augmented secondary reactions. In contrast, it was
411 reported that in a fluidized bed reactor, the recovery of BTEX increased from 1.9 to 6.9 wt.%
412 with the increased temperature from 515 to 628 °C (Park et al., 2020). As a result, the process
413 and apparatus used in the present work have the superiority of producing BTEX at the
414 operating temperature of less than 600 °C. Only at higher operating temperatures of 698 and
415 782 °C, Park et al. obtained a higher BTEX yield (26.3 wt.%) compared to the present work
416 (Park et al., 2020).

Poly-aromatics: The yield of poly-aromatics decreased from 21.6 wt.% at 450 °C (Exp. 5), 21.0 wt.% at 550 °C (Exp. 6) to 15.8 wt.% at 600 °C (Exp. 7) in favor of an increased styrene yield; a similar trend of decreased poly-aromatics with increased temperature was found by Artetxe et al. (Artetxe et al., 2015). Two primary reactions may affect the formation of higher poly-aromatic products: secondary cracking reactions and recombination reactions. The recombination reactions of large radicals increase the yield of poly-aromatic products, whereas the secondary (over-)cracking reactions decrease the yield of higher poly-aromatics products. It should be noted that the elevated temperature increases the secondary (over-)cracking reactions and the termination reactions at different rates. At a certain temperature level (optimum temperature), the rate of the secondary cracking reactions exceeds the rate of the recombination reactions. Subsequently, the formation of poly-aromatic products decreases, as shown in Figure 4. Furthermore, the formation of mono-aromatics such as benzene, toluene, and styrene increased with the increased temperature (Figure 5) which agrees with the findings of Liu et al. (Liu et al., 2000). Finally, the yield of the aliphatic compound was 5.2±1.9 wt.%. The GC × GC analysis confirms that the aliphatic compounds were highly branched and it is likely that polypropylene contamination is the major source of the aliphatic compounds.

3.3.2 Composition of pyrolyzate at reduced pressures (0.02 and 0.5 bara)

The reduced pressure affected the PS pyrolysis yield and enhanced the styrene recovery (see Figure 4 and Table 1). Furthermore, the styrene had the highest concentration at 0.02 bara pressure level compared with the corresponding temperature at the 1.0 bara pressure level. Chauhan et al. pyrolyzed polystyrene at reduced pressure through microwave-assisted pyrolysis and found a similar trend of increased styrene yield at vacuum pressure (Chauhan et

al., 2008). Vacuum minimizes the secondary cracking reactions effect and thus maximizes the primary product styrene due to a shorter $t_{res.}$ in the reactor (see, section 3.2); which is in line with Bartoli et al.'s PS pyrolysis experiments findings (Bartoli et al., 2015). The styrene yield of the mid-point Exp. 4 (500 °C and 0.5 bara) is 41.7 wt.% and it is 2.8 wt.% lower than the average styrene yield of Exp.s 1, 2, 5 and 6 (44.5 wt.%). As such, it appears the effect of pressure on the styrene yield is not completely linear, even though the effect of pressure on the total liquid yield was fairly linear. Moreover, the styrene yield increases with the increased temperature (Figure 4). Likewise, Yang and Shibasaki conducted polystyrene pyrolysis experiments using Py-GC and found an increment of styrene yield with increased temperature (Yang and Shibasaki, 1998). But, beyond the temperature point (550 °C) at which the styrene concentration is maximum (55.9 wt.%), the styrene yield dropped due to enhanced secondary (over-)cracking reactions of intermediate products (Liu et al., 2000). Consequently, the secondary reaction products such as gaseous products (C_1-C_4) increased with the increased temperature (Artetxe et al., 2015). Furthermore, the improvement of styrene concentration at vacuum pressure (0.02 bara) was 14.7 wt.% at (Run 2) 0.02 bara and 550 °C compared to Run 6) 1.0 bara and 550 °C. Besides improving the styrene recovery, the vacuum pressure shifted the temperature point at which the styrene concentration is maximum to the lower level, namely 550 °C. This is could be attributed to the combined effects of pressure and temperature, which could lead to different response rates of the reactions of contrary effects: 1. secondary reactions and 2. depolymerization and β-scission reactions.

Other Mono-aromatics: At vacuum conditions, the yield of other mono-aromatics (excluding styrene) accounts for 9.6±1.3 wt.%, which was lower than the yield at atmospheric pressure at all corresponding temperature levels (450, 550 and 600 °C) (Figure 4). The decreased other

463 mono-aromatics compounds under vacuum is attributed to the shorter $t_{res.}$ which accelerates
464 the removal of primary products and reduces secondary reactions. The yield of other mono-
465 aromatics at the mid-point Exp. 4 is 18.9 wt.% and 1.6 wt.% higher than in experiments 1, 2,
466 6, and 7 (17.3 wt.%).

467 The yield of BTEX increased slightly from 4.3 wt.% at 450 °C (Exp. 5) to peak at 5.6 wt.% at 550
468 °C (Exp. 6) and then decreased to 4.9 wt.% at 600 °C (Exp. 7) (Figure 5); which is in line with
469 Artetxe et al.'s findings on increased single-ring aromatic products (such as toluene,
470 ethylbenzene, and a-methylstyrene) with an increased temperature from 450 to 550 °C, while
471 a further increase above 550 °C led to a decrease in their yield (Artetxe et al., 2015). Similarly,
472 the yield of alpha-methylstyrene changed slightly between 3.2 and 3.4 wt.% (Figure 5). Under
473 vacuum, the BTEX and alpha-methylstyrene yields were reduced compared to atmospheric
474 pressure at the corresponding temperature levels due to the decreased secondary reaction
475 under shorter $t_{res.}$.

476 **Poly-aromatics:** On the one hand, the dimers such as 2,4-Diphenyl-1-butene are formed via
477 1,3-hydrogen transfer reactions followed by mid-chain β-scission reactions (Huang et al.,
478 2020; Levine and Broadbelt, 2008). The dimer compound (2,4-Diphenyl-1-butene) was slightly
479 affected and decreased from 3.8 to 3.7 wt.% with the increased temperature from 450 to 600
480 °C. A similar minor effect of temperature on the dimer formation was found by Artetxe et al.
481 (Artetxe et al., 2015). On the other hand, styrene trimer (2,4,6-triphenyl-1-hexene) is formed
482 via 1,5-hydrogen transfer reactions followed by mid-chain β-scission reactions (Levine and
483 Broadbelt, 2008). And the increased temperature from 450 to 600 °C affected drastically the
484 formation of 2,4,6-triphenyl-1-hexene, which decreased from 12.8 to 0.1 wt.% due to de-
485 polymerization steps and secondary reactions (Artetxe et al., 2015).

The yield of poly-aromatics (higher than di-aromatics and tri-aromatics) decreased from 29.5 wt.% at 450 °C (Exp. 5) to 22.3 wt.% at 550 °C (Exp. 6) and further to 15.2 wt.% at 600 °C (Exp. 7). The yield of poly-aromatics from experiments under vacuum was higher compared to the atmospheric pressure experiments at the corresponding temperature. The vacuum shortens the $t_{res.}$ which minimizes cracking of poly-aromatics compared with atmospheric pressure (Figure 4). The mitigated secondary cracking reactions under vacuum resulted in a smaller amount of other mono-aromatics. Finally, the yield of aliphatic compounds was 5.6±1.6 wt.% which is in the same range as the yield of aliphatic products at atmospheric pressure (Figure 4).

Table 1 summarizes the product yields from pyrolysis of end-of-life PS at the different pressure and temperature levels. In all cases, the gas yield counts less than 4 wt.% and the major products are liquid with a minimum yield of 88.5 wt.%. The impurity of the end-of-life polystyrene feedstock was apparent through detecting heteroatomic compounds in the pyrolyzate such as benzene-acetamide; in contrast, these compounds were not detected in previous works that used virgin or ultra-pure end-of-life PS (Achilias et al., 2007; Artetxe et al., 2015; Park et al., 2020).

In the aim of comparing the effect of feedstock purity on the composition of the pyrolyzate, a virgin PS was processed at 600 °C and 0.02 bara, i.e. under the same operating conditions of Exp. no. 3. The results can be seen in Figure 6.

Processing virgin PS resulted in a styrene yield of 67.1 wt.%, compared to only 54.5 wt.% of styrene in the end-of-life PS pyrolysis case (Figure 6). This is attributed to the differences in feedstock purity, where quantitatively, the contamination of the end-of-life PS feedstock

decreases the net PS in the processed end-of-life PS sample. Furthermore, metallic contaminations such as Mg, Al, Na, and Ca (Roosen et al., 2020b) may affect the pyrolysis process qualitatively. The metallic contaminations play a role as pyrolysis catalyst, which explains the lower liquid pyrolysis yield as found by Iftikhar et al. (Iftikhar et al., 2019). Note that the char formation of end-of-life PS pyrolysis increased by 1.8 wt.% compared to virgin PS pyrolysis case; this behavior can be attributed as well to the metallic contamination contents of the end-of-life PS which favors higher char formation compared to using virgin PS without metallic contaminations (Kabir and Hameed, 2017; Lin et al., 2018). Also, in the end-of-life PS pyrolysis, the mono-aromatics (excluding styrene) yield increased by 4.7 wt.% compared to the virgin PS pyrolysis case because of the metallic contamination's presence and impurities such as PET, PA, and PUR which may decompose into aromatics. The aliphatic compounds yield was 7.1 wt.% higher with end-of-life PS because of the impurity of the feedstock with other plastics types such as polyolefins (Roosen et al., 2020b), whereas no aliphatic compounds were detected in the virgin PS pyrolyzate. The gas products (C_1-C_4) increased slightly from 1.86 wt.% with virgin PS pyrolysis to 2.3 wt.% with end-of-life PS pyrolysis as the feedstock.

3.4 Optimization of pyrolyzate yield and composition

A secondary objective of this study was set to optimize the process conditions depending on the desired product (e.g. styrene versus benzene or dimer yield). Figure 7 (a) shows that the pressure has a limited effect on the liquid pyrolyzate yield, while the temperature increases the liquid pyrolyzate yield up to 94.5 wt.% at 550 °C and 0.02 bara. At higher temperature levels, the liquid pyrolyzate yield decreases again due to secondary and over-cracking reactions that favor gas (C_1-C_4) and char formation (Figure 7 (a)). Note that the contour plot

of liquid pyrolyzate can be used as a guideline to calculate the cost of pyrolyzate production depending on the operating cost at varied pressure and temperature levels. Moreover, the optimum operating conditions of the pyrolyzate liquid yield could differ from the optimum operating conditions for styrene. Figure 7 (b) shows that the styrene yield reaches maxima between 550 and 575 °C at 0.02 bara with a styrene yield of 56 wt.%. Higher pressure (1.0 bara) and lower temperatures (450 °C) decrease the styrene yield substantially, to less than 36 wt.% (Figure 7 (b)). The pressure has no actual effect on the liquid yield but a large effect on the styrene concentration (Figure 7 (a, b)). The yield of benzene, toluene, ethylbenzene, and xylenes (BTEX) vary between 8.4 and 27.6 wt.% (Figure 7 (c)). In the studied pressure and temperature ranges, the pressure has a more pronounced effect compared to the temperature on the yield of BTEX.

Figure 7 (d) shows the ratio of styrene to BTEX (St./BTEX) at different pressure and temperature levels. This parameter can be used to tune the process based on the market requirements and/or the installation and operating costs of the distillation equipment. The lowest ratio of St./BTEX (1.6) was obtained at a 1.0 bara pressure level and temperature level of 500 °C. The St./BTEX ratio increased up to 5.6 with increased temperature in the range of 560 °C and 600 °C and lower pressure (0.02 bara).

The yield of trimers and dimers can be optimized depending on the industrial and market conditions as well. The dimer and trimer yield increased with increased pressure and temperature (Figure 7 (e)) and varied in the range of 5 to 17 wt.%. Both increased pressure and temperature reduced the yield of dimers and trimers due to the increased $t_{res.}$ with increased pressure and augmented secondary cracking reactions. Finally, the yield of higher poly-aromatics excluding di-aromatics and tri-aromatics is shown in (Figure 7 (f)). The minimal

554 yield of this fraction is at a higher temperature level of 600 °C at both pressure levels from
555 0.02 to 1.0 bara, which is attributed to the shorter $t_{res.}$ and the dominance of the secondary
556 cracking reaction. The obtained results can be used as an input for a comprehensive techno-
557 economical assessment. Moreover, the process of PS pyrolysis can be further optimized based
558 on the target components and feedstock purity. As mentioned earlier, an increase in
559 temperature and decrease in pressure enhances the devolatilization and de-propagation
560 reactions.

561 4 Conclusion

562 The continuous pyrolysis process of end-of-life PS was studied in a vacuum and atmospheric
563 pressure in a continuous stirred tank reactor (CSTR). A maximum yield of benzene, toluene,
564 ethylbenzene, and xylene BTEX (17.1 wt.%) was observed at 450 °C and 1.0 bara, which
565 corresponds to a lower temperature for a similar yield of PS pyrolysis in a fluidized bed reactor.
566 At the pressure level of 0.02 bara, the maximum yield of styrene (55.9 wt.%) was achieved at
567 550 °C which was considered to be the temperature point of maximum yield; beyond of this
568 optimal point, the styrene yield decreased. Compared to the atmospheric pressure level, the
569 vacuum pressure decreased the temperature point from 600 °C to 550 °C which is
570 economically favorable due to lower energy consumption to pyrolyze the PS.

571 The operating pressure and temperature affected the product distribution in the studied
572 ranges of 450-600 °C and 0.02-1.0 bara, but in these ranges, the temperature had a more
573 pronounced effect. The GC × GC-FID and GC × GC-TOF/MS analyses led to a detailed
574 characterization of the polystyrene pyrolyzate. Interestingly, feedstock impurities and
575 contaminations could be qualified by detecting unique pyrolysis product compounds such as

2, 4, 6, 8-tetramethyl-1-undecene, which is a characteristic compound of polypropylene pyrolysis. The latter was an indication that PP was a contaminant of end-of-life PS stream. These analyses results show the superiority and necessity of using GC × GC for analyzing a complex contaminated end-of-life PS pyrolyzate and to avoid overlapping of compounds' peaks. A higher purity feedstock led to higher styrene yield, with styrene being the most valuable PS pyrolyzate product. On the other hand, further purification of the end-of-life PS would potentially increase the cost of pre-processing and treatments; therefore, a techno-economical assessment is required to maximize the styrene yield with minimal pre-treatment cost. To ensure the quality and purity of the end-of-life plastic feedstock, comprehensive GC × GC analysis or fast screening methods based on pyrolysis GC can be used to analyze the liquid pyrolysis products of these feedstocks. Since the post-processing and distillation of the liquid pyrolyzate result poly-aromatics cuts that contain dimers and trimers, further studies are therefore necessary to clarify the potential of re-pyrolyzing of the poly-aromatics cuts to produce styrene and BTEX. Measuring the heat input of the extruder and the energy consumption of the auxiliary equipment will help in performing a comprehensive techno-economical assessment. In addition, the research on removing end-of-life PS contaminants by pre-processing steps can be planned for future work. Finally, the presented results for pyrolysis of end-of-life PS can be used as a basis for scale-up to an industrial-sized plant.

Acknowledgments

This work was supported by Flanders Innovation & Entrepreneurship (VLAIO) and the O&O project "Thermochemical Conversion of End-of-Life Plastics to Chemical Feedstock"; (Nederlandse vertaling: Thermochemische Omzetting van End-of-Life Kunststoffen tot Chemische Feedstocks). The research leading to these results has also received funding from

the Fund for Scientific Research Flanders (FWO) and innovation program/ERC grant agreement no.818607 (OPTIMA).

Declaration of competing interest

The authors declare no conflict of interest.

CRediT authorship contribution statement

Azd Zayoud: conceptualization, methodology, investigation, writing – original draft, writing – review & editing. **Hang Dao Thi**: investigation, writing – review & editing. **Marvin Kusenberg**: methodology, investigation, writing – review & editing. **Andreas Eschenbacher**: writing – review & editing. **Uros Kresovic**: resources, review & editing. **Nick Alderweireldt**: resources, review & editing. **Marko Djokic**: methodology, investigation, writing – review & editing. **Kevin M. Van Geem**: conceptualization, funding acquisition, project administration, supervision, writing – review & editing.

References

Achilias, D.S., Kanellopoulou, I., Megalokonomos, P., Antonakou, E., Lappas, A.A., 2007. Chemical Recycling of Polystyrene by Pyrolysis: Potential Use of the Liquid Product for the Reproduction of Polymer. Macromol Mater Eng 292, 923-934, https://doi.org/10.1002/mame.200700058.

Agilyx, 2020. Driving innovations to make plastics a renewable resource.

Akima, H., 1970. A New Method of Interpolation and Smooth Curve Fitting Based on Local Procedures. J Acm 17, 589-602, https://doi.org/10.1145/321607.321609.

Akima, H., 1974. A method of bivariate interpolation and smooth surface fitting based on local procedures. Communications of the ACM 17, 18-20, https://doi.org/10.1145/360767.360779.

Akima, H., 1978. A Method of Bivariate Interpolation and Smooth Surface Fitting for Irregularly Distributed Data Points. ACM Transactions on Mathematical Software 4, 148-159, https://doi.org/10.1145/355780.355786.

Ando, H., Inomata, O., Abe, T., Matsuzawa, S., Shimizu, Y., Miyazaki, S., 1974. Pyrolysis of Plastic Wastes (I). Journal of the Fuel Society of Japan 53, 646-653, https://doi.org/10.3775/jie.53.7_646.

Artetxe, M., Lopez, G., Amutio, M., Barbarias, I., Arregi, A., Aguado, R., Bilbao, J., Olazar, M., 2015. Styrene recovery from polystyrene by flash pyrolysis in a conical spouted bed reactor. Waste Manag 45, 126-133, https://doi.org/10.1016/j.wasman.2015.05.034.

Bartoli, M., Rosi, L., Frediani, M., Undri, A., Frediani, P., 2015. Depolymerization of polystyrene at reduced pressure through a microwave assisted pyrolysis. Journal of Analytical and Applied Pyrolysis 113, 281-287, https://doi.org/10.1016/j.jaap.2015.01.026.

Beens, J., Boelens, H., Tijssen, R., Blomberg, J., 1998. Quantitative Aspects of Comprehensive Two-Dimensional Gas Chromatography (GC×GC). Journal of High Resolution Chromatography 21, 47-54.

Beens, J., Janssen, H.G., Adahchour, M., Brinkman, U.A., 2005. Flow regime at ambient outlet pressure and its influence in comprehensive two-dimensional gas chromatography. J Chromatogr A 1086, 141-150, https://doi.org/10.1016/j.chroma.2005.05.086.

Brooks, A.L., Wang, S., Jambeck, J.R., 2018. The Chinese import ban and its impact on global plastic waste trade. Sci Adv 4, eaat0131, https://doi.org/10.1126/sciadv.aat0131.

Chauhan, R.S., Gopinath, S., Razdan, P., Delattre, C., Nirmala, G.S., Natarajan, R., 2008. Thermal decomposition of expanded polystyrene in a pebble bed reactor to get higher liquid fraction yield at low temperatures. Waste Manag 28, 2140-2145, https://doi.org/10.1016/j.wasman.2007.10.001.

Dalluge, J., van Rijn, M., Beens, J., Vreuls, R.J., Brinkman, U.A., 2002. Comprehensive two-dimensional gas chromatography with time-of-flight mass spectrometric detection applied to the determination of pesticides in food extracts. J Chromatogr A 965, 207-217, https://doi.org/10.1016/s0021-9673(01)01324-3.

Dijkmans, T., Djokic, M.R., Van Geem, K.M., Marin, G.B., 2015. Comprehensive compositional analysis of sulfur and nitrogen containing compounds in shale oil using GC×GC – FID/SCD/NCD/TOF-MS. Fuel 140, 398-406, https://doi.org/10.1016/j.fuel.2014.09.055.

Djokic, M., Carstensen, H.-H., Van Geem, K.M., Marin, G.B., 2013. The thermal decomposition of 2,5-dimethylfuran. Proceedings of the Combustion Institute 34, 251-258, https://doi.org/10.1016/j.proci.2012.05.066.

Djokic, M.R., Ristic, N.D., Olahova, N., Marin, G.B., Van Geem, K.M., 2017. Quantitative on-line analysis of sulfur compounds in complex hydrocarbon matrices. J Chromatogr A 1509, 102-113, https://doi.org/10.1016/j.chroma.2017.06.006.

Doucet, J., 2020. The Endless Regeneration of Plastics Through Microwaves.

Doucet, J., Chaouki, J., Sobhy, A., 2016. Catalyst for distributed batch microwave pyrolysis, system and process thereof.

Garside, M., 2019. Global plastic production from 1950 to 2018 (in million metric tons).

Huang, J., Li, X., Meng, H., Tong, H., Cai, X., Liu, J., 2020. Studies on pyrolysis mechanisms of syndiotactic polystyrene using DFT method. Chemical Physics Letters 747, https://doi.org/10.1016/j.cplett.2020.137334.
Iftikhar, H., Zeeshan, M., Iqbal, S., Muneer, B., Razzaq, M., 2019. Co-pyrolysis of sugarcane bagasse and polystyrene with ex-situ catalytic bed of metal oxides/HZSM-5 with focus on liquid yield. Bioresour Technol 289, 121647, https://doi.org/10.1016/j.biortech.2019.121647.
Kabir, G., Hameed, B.H., 2017. Recent progress on catalytic pyrolysis of lignocellulosic biomass to high-grade bio-oil and bio-chemicals. Renewable and Sustainable Energy Reviews 70, 945-967, https://doi.org/10.1016/j.rser.2016.12.001.
Kaminsky, W., 2021. Chemical recycling of plastics by fluidized bed pyrolysis. Fuel Communications 8, https://doi.org/10.1016/j.jfueco.2021.100023.
Kaminsky, W., Franck, J., 1991. Monomer recovery by pyrolysis of poly(methyl methacrylate) (PMMA). Journal of Analytical and Applied Pyrolysis 19, 311-318, https://doi.org/10.1016/0165-2370(91)80052-a.
Kaminsky, W., Predel, M., Sadiki, A., 2004. Feedstock recycling of polymers by pyrolysis in a fluidised bed. Polymer Degradation and Stability 85, 1045-1050, https://doi.org/10.1016/j.polymdegradstab.2003.05.002.
Karaduman, A., Şimşek, E.H., Çiçek, B., Bilgesü, A.Y., 2001. Flash pyrolysis of polystyrene wastes in a free-fall reactor under vacuum. Journal of Analytical and Applied Pyrolysis 60, 179-186, https://doi.org/10.1016/s0165-2370(00)00169-8.
Kim, Y.S., Hwang, G.C., Bae, S.Y., Yi, S.C., Moon, S.K., Kumazawa, H., 1999. Pyrolysis of polystyrene in a batch-type stirred vessel. Korean J Chem Eng 16, 161-165, https://doi.org/10.1007/bf02706830.
Levine, S.E., Broadbelt, L.J., 2008. Reaction pathways to dimer in polystyrene pyrolysis: A mechanistic modeling study. Polymer Degradation and Stability 93, 941-951, https://doi.org/10.1016/j.polymdegradstab.2008.01.029.
Lin, X., Zhang, Z., Zhang, Z., Sun, J., Wang, Q., Pittman, C.U., 2018. Catalytic fast pyrolysis of a wood-plastic composite with metal oxides as catalysts. Waste Manag 79, 38-47, https://doi.org/10.1016/j.wasman.2018.07.021.
Liu, Y., Qian, J., Wang, J., 2000. Pyrolysis of polystyrene waste in a fluidized-bed reactor to obtain styrene monomer and gasoline fraction. Fuel Processing Technology 63, 45-55, https://doi.org/10.1016/s0378-3820(99)00066-1.
Madorsky, S., Straus, S., 1948. Pyrolytic fractionation of polystyrene in a high vacuum and mass spectrometer analysis of some of the fractions. Journal of research of the National Bureau of Standards 40, 417-425.
Madorsky, S.L., 1952. Rates of thermal degradation of polystyrene and polyethylene in a vacuum. Journal of Polymer Science 9, 133-156, https://doi.org/10.1002/pol.1952.120090203.
Mo, Y., Zhao, L., Wang, Z., Chen, C.L., Tan, G.Y., Wang, J.Y., 2014. Enhanced styrene recovery from waste polystyrene pyrolysis using response surface methodology coupled with Box-Behnken design. Waste Manag 34, 763-769, https://doi.org/10.1016/j.wasman.2014.01.005.
Murata, K., Hirano, Y., Sakata, Y., Uddin, M.A., 2002. Basic study on a continuous flow reactor for thermal degradation of polymers. Journal of Analytical and Applied Pyrolysis 65, 71-90, https://doi.org/10.1016/s0165-2370(01)00181-4.
Murata, K., Sato, K., Sakata, Y., 2004. Effect of pressure on thermal degradation of polyethylene. Journal of Analytical and Applied Pyrolysis 71, 569-589, https://doi.org/10.1016/j.jaap.2003.08.010.
Ogino, H., Nagy, B., 1981. Pyrolysis of Transvaal kerogens. II. An evaluation of vacuum pyrolysis with polyethylene, polystyrene and their mixtures with minerals. Precambrian Research 15, 113-130, https://doi.org/10.1016/0301-9268(81)90025-5.
Park, J.J., Park, K., Kim, J.-S., Maken, S., Song, H., Shin, H., Park, J.-W., Choi, M.-J., 2003. Characterization of Styrene Recovery from the Pyrolysis of Waste Expandable Polystyrene. Energy & Fuels 17, 1576-1582, https://doi.org/10.1021/ef030102l.

Park, K.-B., Jeong, Y.-S., Guzelciftci, B., Kim, J.-S., 2020. Two-stage pyrolysis of polystyrene: Pyrolysis oil as a source of fuels or benzene, toluene, ethylbenzene, and xylenes. Appl Energ 259, https://doi.org/10.1016/j.apenergy.2019.114240.
Phillips, J.B., Beens, J., 1999. Comprehensive two-dimensional gas chromatography: a hyphenated method with strong coupling between the two dimensions. Journal of Chromatography A 856, 331-347, https://doi.org/10.1016/s0021-9673(99)00815-8.
PlasticsEurope, 2018. Plastics the facts 2018.
PlasticsEurope, 2019a. Plastics 2030 PlasticsEurope's Voluntary Commitment to increasing circularity and resource efficiency.
PlasticsEurope, 2019b. Plastics the facts 2019.
PolystyreneLoop, 2021. PolyStyreneLoop project: pioneer demonstration plant to treat up to 3300 tonnes of polystyrene waste/yr as of 2018.
Pyrolyze.B.V., 2021. 150 kg/h plastic pyrolysis plant.
Qureshi, K.M., Kay Lup, A.N., Khan, S., Abnisa, F., Wan Daud, W.M.A., 2018. A technical review on semi-continuous and continuous pyrolysis process of biomass to bio-oil. Journal of Analytical and Applied Pyrolysis 131, 52-75, https://doi.org/10.1016/j.jaap.2018.02.010.
Qureshi, M.S., Oasmaa, A., Lindfors, C., 2019. <Thermolysis of plastic waste_ Reactor comparison.pdf>, in: Berruti, F., Dufour, A., Prins, W., Garcia-Pérez, M. (Eds.), Pyroliq 2019: Pyrolysis and Liquefaction of Biomass and Wastes, Cork, Ireland
Roosen, M., Mys, N., Kusenberg, M., Billen, P., Dumoulin, A., Dewulf, J., Van Geem, K.M., Ragaert, K., De Meester, S., 2020a. Detailed Analysis of the Composition of Selected Plastic Packaging Waste Products and Its Implications for Mechanical and Thermochemical Recycling. Environ. Sci. Technol. 54, 13282-13293, https://doi.org/10.1021/acs.est.0c03371.
Roosen, M., Mys, N., Kusenberg, M., Billen, P., Dumoulin, A., Dewulf, J., Van Geem, K.M., Ragaert, K., De Meester, S., 2020b. Detailed Analysis of the Composition of Selected Plastic Packaging Waste Products and Its Implications for Mechanical and Thermochemical Recycling. Environ Sci Technol 54, 13282-13293, https://doi.org/10.1021/acs.est.0c03371.
Smalley, M., 2019. Agilyx partners to launch European PS chemical recycling plant: Styrenics Circular Solutions, Agilyx aim to develop a commercial-scale chemical recycling plant. www.recyclingtoday.com.
Soják, L., Kubinec, R., Jurdáková, H., Hájeková, E., Bajus, M., 2007. High resolution gas chromatographic–mass spectrometric analysis of polyethylene and polypropylene thermal cracking products. Journal of Analytical and Applied Pyrolysis 78, 387-399, https://doi.org/10.1016/j.jaap.2006.09.012.
Toraman, H.E., Dijkmans, T., Djokic, M.R., Van Geem, K.M., Marin, G.B., 2014. Detailed compositional characterization of plastic waste pyrolysis oil by comprehensive two-dimensional gas-chromatography coupled to multiple detectors. J Chromatogr A 1359, 237-246, https://doi.org/10.1016/j.chroma.2014.07.017.
Undri, A., Frediani, M., Rosi, L., Frediani, P., 2014. Reverse polymerization of waste polystyrene through microwave assisted pyrolysis. Journal of Analytical and Applied Pyrolysis 105, 35-42, https://doi.org/10.1016/j.jaap.2013.10.001.
Victory, M., 2020. INEOS, Plastic Energy to build pyrolysis-based chemical recycling plant.
Williams, P.T., Williams, E.A., 2010. Product Composition from the Fast Pyrolysis of Polystyrene. Environmental Technology 20, 1109-1118, https://doi.org/10.1080/09593332008616908.
Yang, M., Shibasaki, Y., 1998. Mechanisms of thermal degradation of polystyrene, polymethacrylonitrile, and their copolymers on flash pyrolysis. Journal of Polymer Science Part A: Polymer Chemistry 36, 2315-2330.

Figures and tables

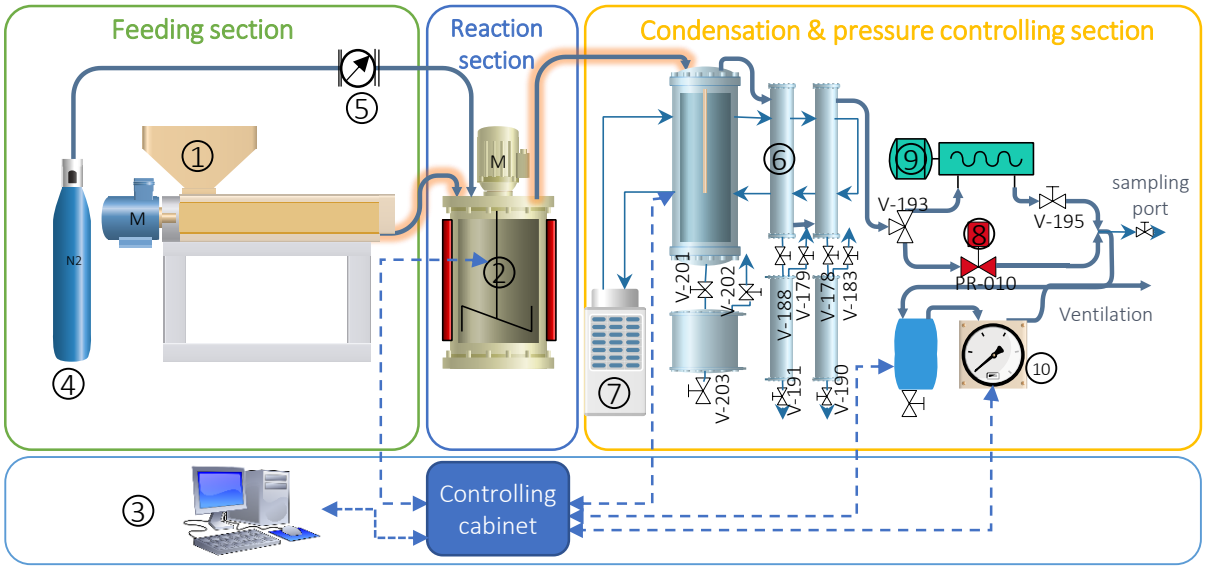

Figure 1 Flow diagram of the pyrolysis pilot unit: (1) extruder, (2) CSTR, (3) controlling cabinet, and PC, (4) N_2 cylinder, (5) N_2 volumetric flow controller, (6) condensers, (7) cooler, (8) back pressure controller, (9) vacuum pump, (10) off-gas flowmeter

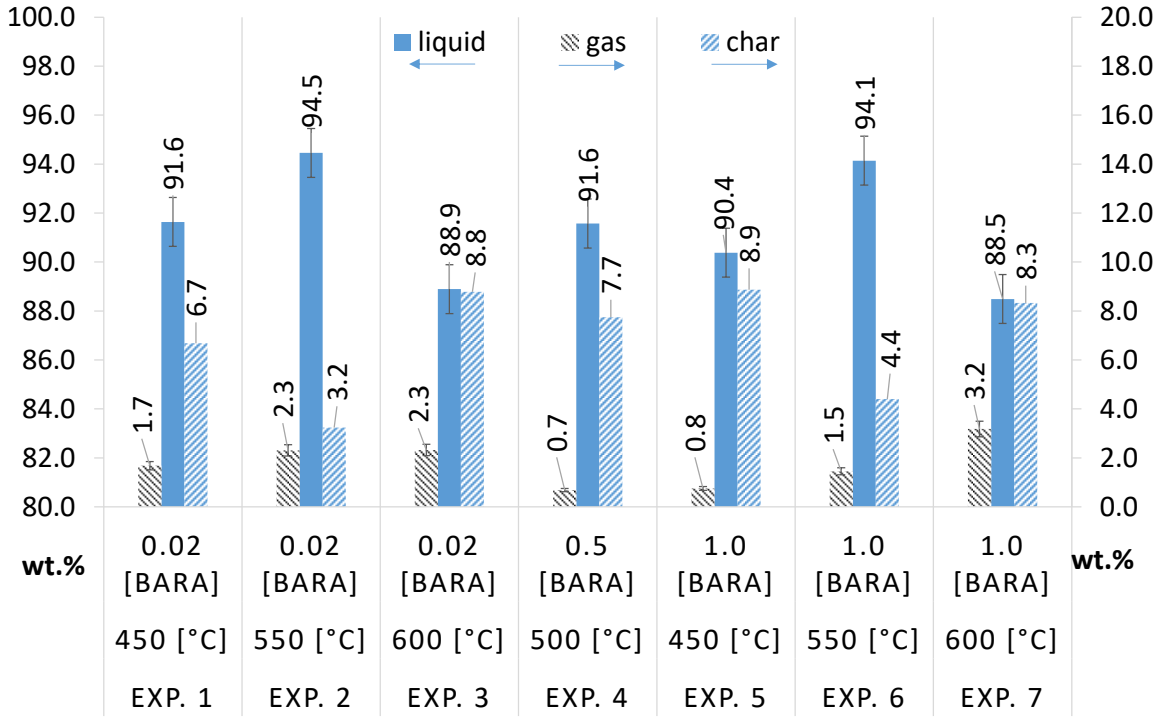

Figure 2 The mass balance of the continuous polystyrene pyrolysis in CSTR

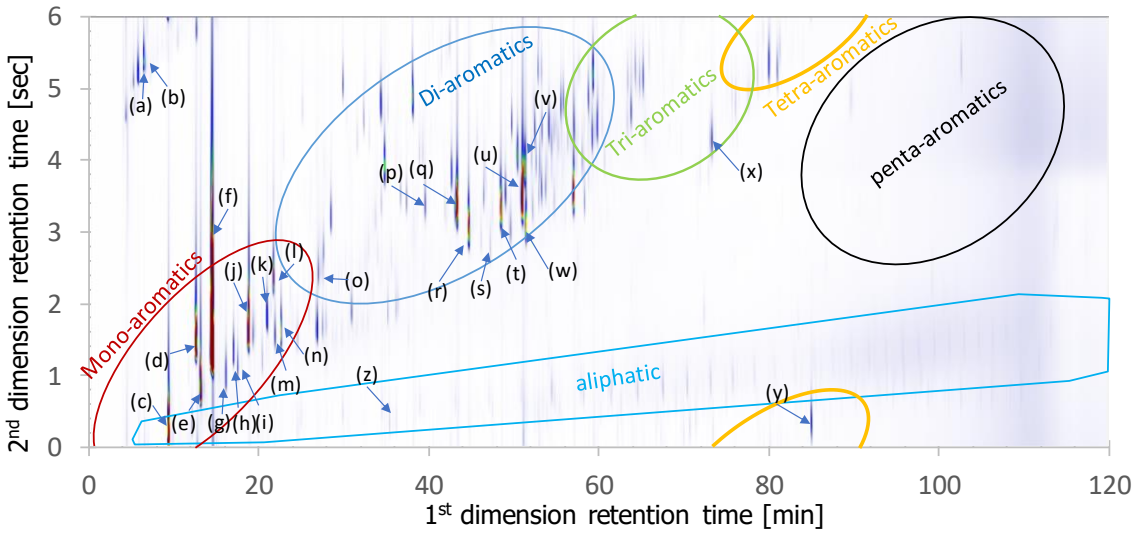

*Figure 3 GC × GC – FID chromatogram of the end-of-life polystyrene pyrolyzate with major compounds and group types. **(a)** Benzene **(b)** Cyclohexane **(c)** Toluene **(d)** IS=3-chlorothiophene **(e)** Ethylbenzene **(f)** Styrene **(g)** 1,2,4 trimethylbenzene **(h)** Benzene, 1-ethenyl-2-methyl- **(i)** Benzene, propyl- **(j)** Alpha-methylstyrene **(k)** Benzene, 1-ethenyl-2-methyl- **(l)** Indene **(m)** Benzene, 3-butenyl- **(n)** Benzene, (1-methylenepropyl) **(o)** Naphthalene **(p)** Diphenylmethane **(q)** Bibenzyl **(r)** 1,2-Diphenylpropane **(s)** 2,5-Diphenyl-2-hexene **(t)** 1,3-Diphenylpropane **(u)** 2,4-Diphenyl-1-butene **(v)** 1,3-Diphenylpropene **(w)** 2,4-Diphenyl-1-pentene **(x)** 2,4,6-triphenyl-1-hexene **(y)** 1,2,4-Triphenylbenzene **(z)** 2, 4, 6, 8-tetramethyl-1-undecene.*

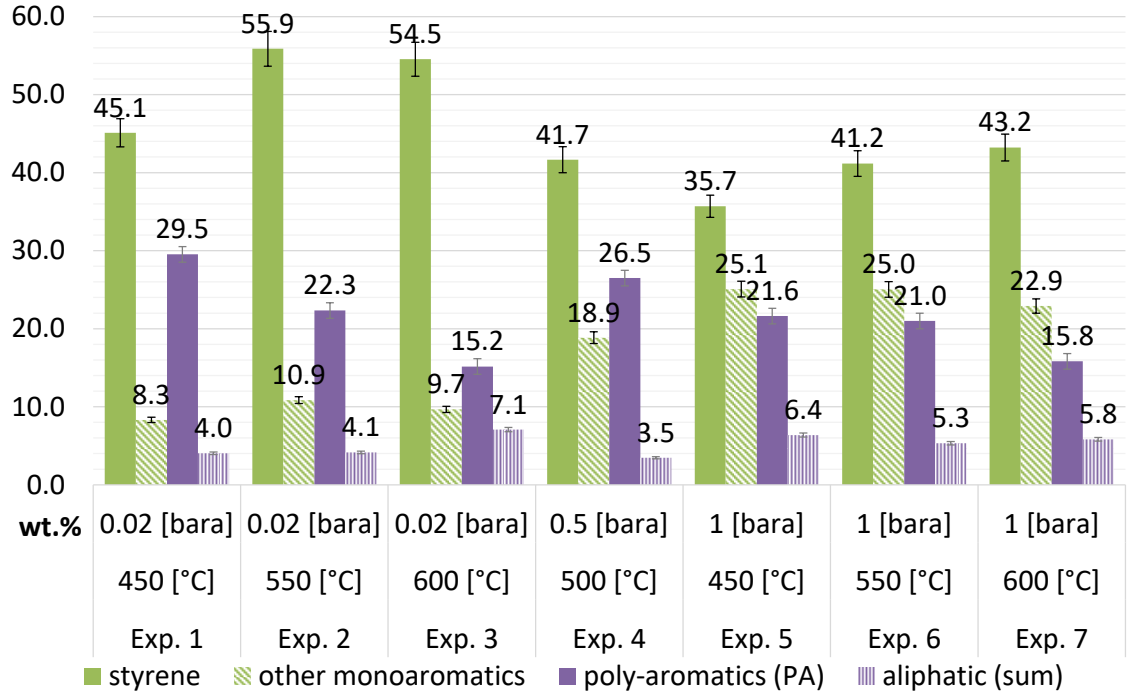

Figure 4 Effect of temperature (450, 500, 550 and 600 °C) and pressure (0.02, 0.5 and 1.0 bara) on the yield (wt.%) of the four main product groups found in polystyrene pyrolyzate

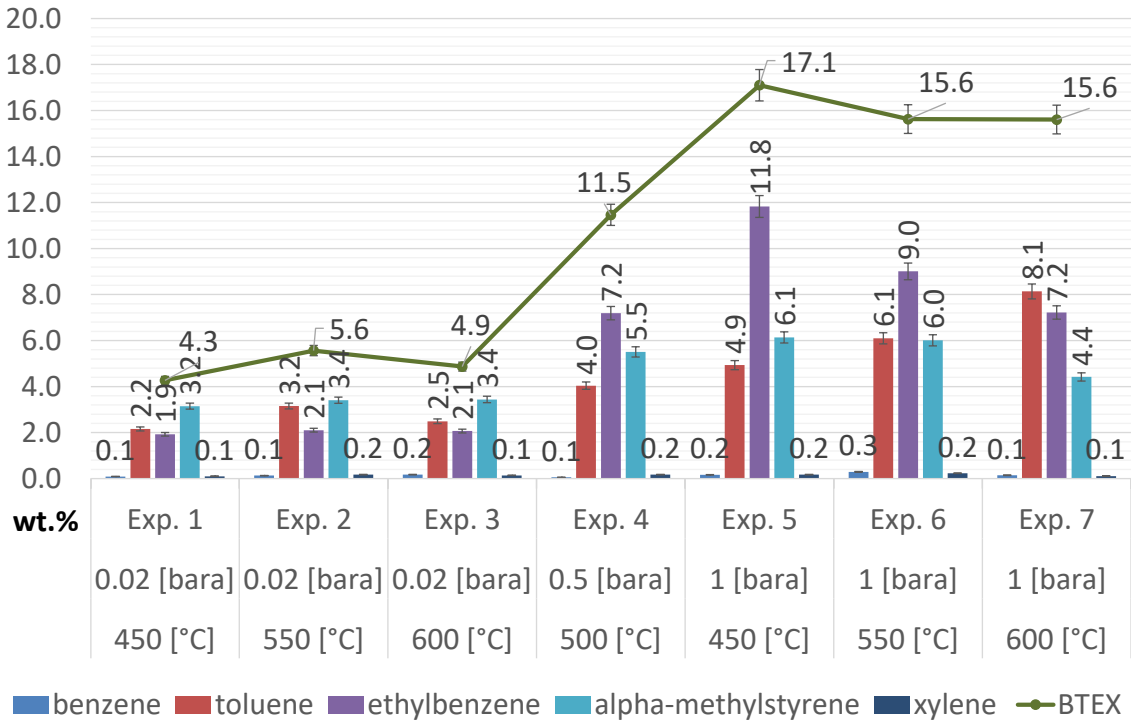

775

776 *Figure 5 Effect of temperature and pressure on the formation of BTEX and mono-aromatics excluding*
777 *styrene.*

778 *Table 1 Yield (wt.%) of products from pyrolysis of end-of-life polystyrene (mono-aromatics (mon-A),*
779 *di-aromatics (di-A), tri-aromatics tri-A), tetra-aromatics (tetra-A),)*

Experiment			1	2	3	4	5	6	7
P [bara]			0.02	0.02	0.02	0.5	1.00	1.00	1.00
T [°C]			450	550	600	500	450	550	600
Compound Name	Group type	C#	wt.% to the input feedstock						
gas (sum)	C1-C4		1.7	2.3	2.3	0.7	0.8	1.5	3.2
Liquid (sum)			91.6	94.5	88.9	91.6	90.4	94.1	88.5
toluene	mon-A	7	2.2	3.2	2.5	4.0	4.9	6.1	8.1
ethylbenzene	mon-A	8	1.9	2.1	2.1	7.2	11.8	9.0	7.2
styrene	mon-A	8	45.1	55.9	54.5	41.7	35.7	41.2	43.2
alpha-methylstyrene	mon-A	9	3.2	3.4	3.4	5.5	6.1	6.0	4.4
other mono.A	mon-A		1.1	2.2	1.7	2.1	2.2	3.9	3.1
1,3-Diphenylpropane	di-A	15	2.2	1.4	0.9	3.5	4.3	2.8	1.6
1,3-Diphenylpropene	di-A	15	0.4	0.5	0.5	0.9	0.9	0.7	0.5
2,4-Diphenyl-1-butene (dimer)	di-A	16	3.8	3.3	3.7	2.4	1.3	1.0	0.4
other di-A	di-A		4.5	9.2	8.5	7.9	6.4	10.0	9.8
C24H24 tri-A	tri-A	24	1.6	1.3	0.3	1.7	0.9	1.3	0.4
2,4,6-triphenyl-1-hexene (trimer)	tri-A	24	12.8	1.8	0.1	1.9	2.4	0.1	0.9
C25H26 tri-A	tri-A	25	0.7	1.2	0.1	1.4	0.9	0.7	0.2

other tri-A	tri-A	3.1	2.0	0.5	2.6	1.8	2.6	1.2
other tetra-A	tetra-A	0.5	1.7	0.5	4.0	2.6	1.7	0.9
aliphatic (sum)	aliphatic	4.0	4.1	7.1	3.5	6.4	5.3	5.8
others	others	4.7	1.2	2.5	1.1	1.6	1.6	0.7
char		6.7	3.2	8.8	7.7	8.9	4.4	8.3
total (yield to the input)		100.0	100.0	100.0	100.0	100.0	100.0	100.0

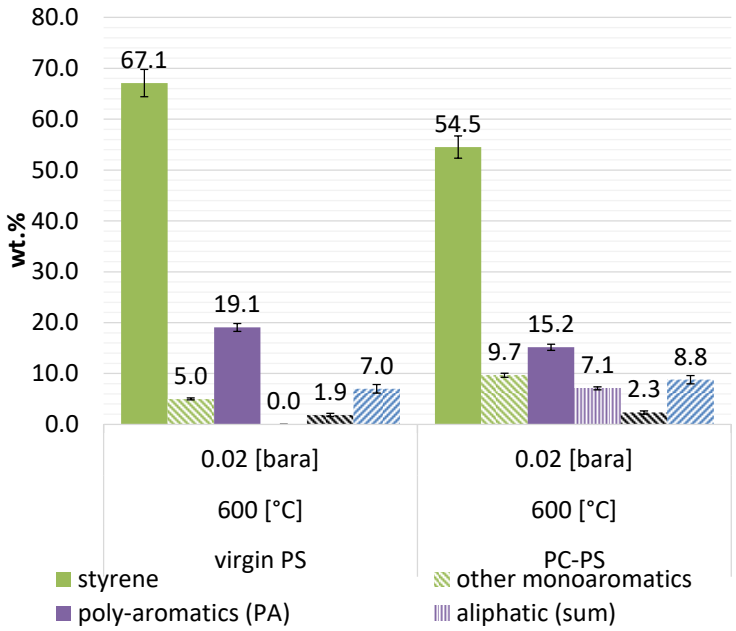

780

781 *Figure 6 Comparison of product distribution using virgin PS and end-of-life PS as feed at pyrolysis*
782 *conditions of 600 °C and 0.02 bara*

783

784

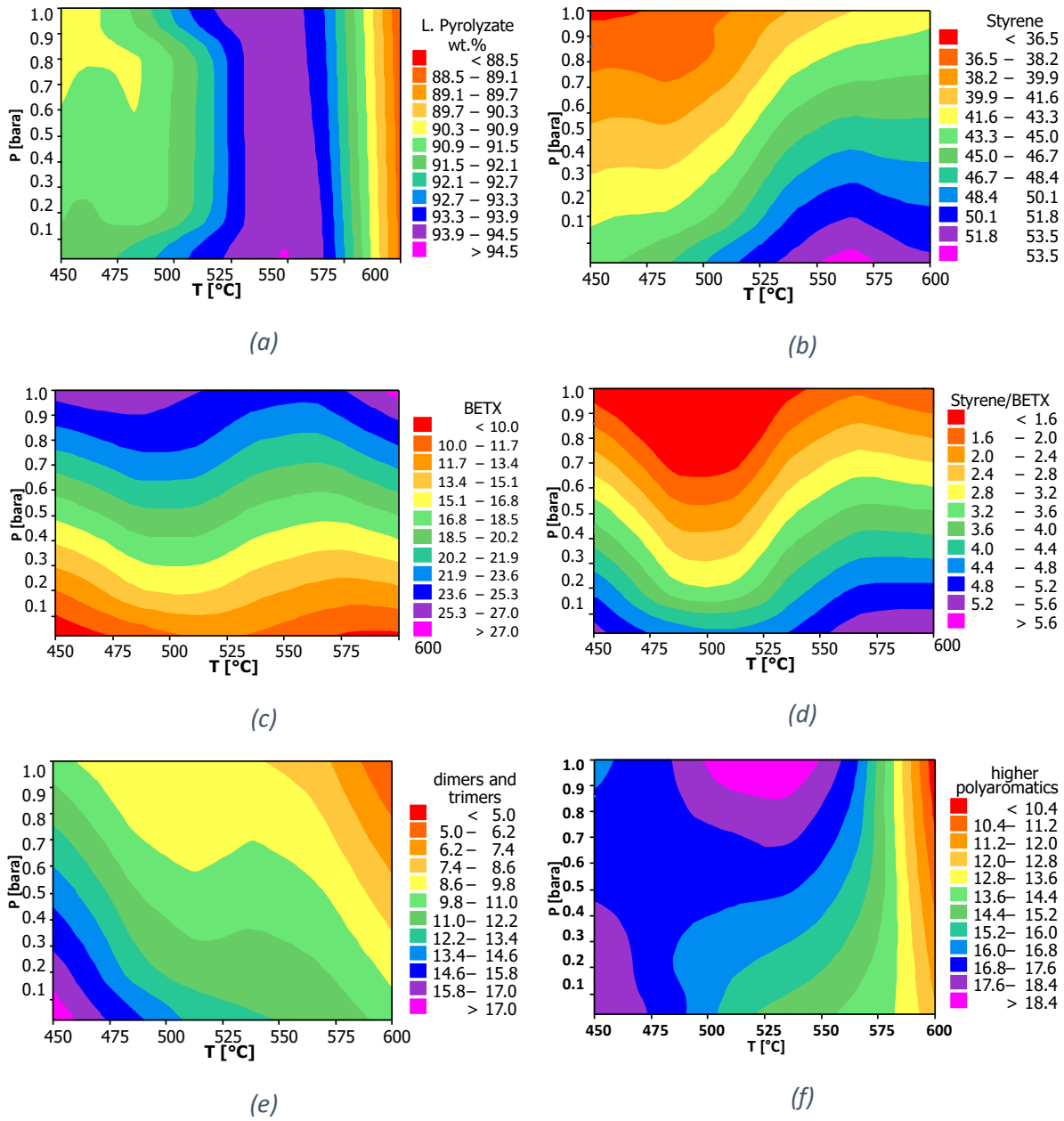

*Figure 7 Product yield contour plot [wt.%] versus pressure [bara] and temperature [°C], **(a)** The contour plot of liquid pyrolyzate [wt.%] versus p and T, **(b)** The contour plot of styrene yield versus P and T, **(c)** The contour plot of (BTEX) yield [wt.%] versus P and T, **(d)** The contour plot of the ratio of styrene to BTEX versus P and T, (e) The contour plot of dimers and trimers [wt.%] versus P and T, (f) The contour plot of higher poly-aromatics [wt.%] versus P and T*

785